Vibration Suppression of a Slotless Self-Bearing Permanent-Magnet Motor for Optical Applications

Elias Doenni [†], Timon Achtnich [a], Christof Zwyssig [a]

***Abstract*— Magnetic bearings, particularly of slotless type, are ideally suited for optical applications by enabling operation in vacuum at high speeds with high lifetime, avoiding particle generation and allowing active control, and therefore suppression of bearing stator force and rotor displacements. In this paper, different approaches for vibration suppression are compared and experimentally verified with a dual hetero-/homopolar slotless self-bearing motor. A feed forward has advantages compared to a notch-filter approach as it allows rotor vibration suppression and lowering the stator vibration suppression activation speed into the rigid-rotor critical speed range. Finally, the rotational speed fluctuations, important for optical applications, are investigated.**

I. Introduction

Magnetic bearings are ideally suited for optical applications, by enabling operation in vacuum, avoiding particle generation and, particularly with a slotless bearing and motor topology as presented in [1], featuring high-speed capability combined with a high lifetime. A further advantage of active magnetic bearings is the possibility to actively suppress undesired bearing forces and rotor displacements, in the following called vibrations, which is beneficial or required in many optical applications. Stator vibrations have to be limited if vibration propagation into neighbouring optical systems has to be avoided, e.g. in laser applications [2] or for reaction-wheels used for attitude control in satellites requiring high spacecraft pointing accuracy [1], [3]. Other applications, like rotating polygon scanners for biomedical applications or high repetition-rate lasers with high pulse energy, require high beam pointing- and speed accuracy and hence minimal rotor vibrations, high rotational speed stability or even synchronization with an external trigger source [4].

Therefore, in this paper different methods to suppress stator and rotor vibrations in a slotless self-bearing motor are investigated and experimentally validated.

II. Slotless Self-Bearing Motor

The dual hetero-/homopolar slotless self-bearing motor developed in [1] is depicted in Figure 1. Drive torque and radial bearing forces are generated by the heteropolar motor, while radial and axial bearing forces are generated by the homopolar motor. A radially magnetized permanent magnet is embedded in the rotor sleeve on the heteropolar rotor side, while two axially-magnetized magnets are employed in the homopolar rotor side.

To allow for closed-loop control of all six degrees of freedom of the rotor, the radial rotor positions are measured by means of eddy-current sensors in both bearings, while additional hall sensors in the heteropolar motor are used for measurement of the axial rotor position and the rotor angle.

[a]Celeroton AG, Industriestrasse 22, 8604 Volketswil, Switzerland, corresponding author: Christof Zwyssig: christof.zwyssig@celeroton.com
[†]Deceased June 2018

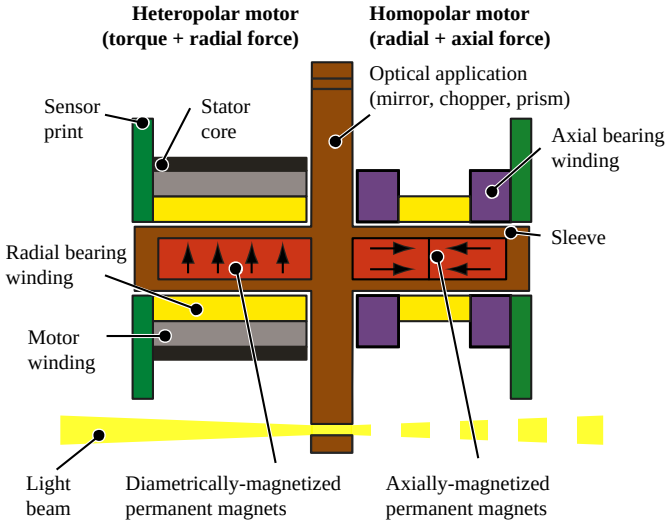

Figure 1. Dual hetero-/homopolar slotless self-bearing motor with optical chopper disc rotor.

The motor allows to reach rotational speeds up to 400 krpm, depending on the rotor geometry.

III. Suppression of Stator Vibrations

The basic idea of stator vibration suppression is to allow the rotor to spin around its axis of inertia by allowing Ω-synchronous rotor displacements due to unbalance, such that no unbalance forces appear. The applicability of this feature is unique to magnetic bearings and has been described extensively [5], [6], [7].

A. Notch Filter

Typically, a notch filter tuned to rotational frequency is used for unbalance force rejection [5], [6]. However, control stability is affected when applying the notch filter to the measured rotor position while operating near rigid-rotor critical frequencies (below 10 krpm for the described motor, cf. Figure 3). Unbalance forces excite resonances which are no longer damped by the position controller, hence the poles of nutation, precession and pendulous vibration become unstable.

Another interpretation is that the notch filter must not be enabled in the frequency range of the bandwidth of the position controller, as the notch is adding a negative phase of 90 degrees below its resonance frequency.

In practical applications, the activation speed of the notch filter must be sufficiently higher than the critical frequencies to ensure robust stability, i.e. above 30 krpm for the described motor.

B. Feed forward

For above reasons, an additive compensation approach is applied to allow for stator vibration suppression also below the activation speed threshold of the notch filter.

The idea is to use an additive instead of a multiplicative filtering, i.e only Ω-synchronous rotor displacements due to

unbalance are subtracted from the measured position (cf. Figure 4). This compensation can therefore be interpreted as generalized notch filter with a limited attenuation: Ω-synchronous displacements exceeding the rotor eccentricity are not filtered and nutation, precession and pendulous vibration are still damped by the position controller. The closed-loop transfer function and hence closed-loop stability are unaffected by the stator vibration compensation.

The orbit of the rotor position at high rotational speeds, when the rotor is rotating around its axis of inertia, can be used as initial value for the compensation terms. The optimal amplitude and phase of the compensation position

$$Y_c = A_c \sin(\gamma + \varphi_c) \tag{1}$$

can be found by iterative minimization of the rotational-frequency component of the stator currents

$$Y_{c,opt} = \underset{Y_c}{\operatorname{argmin}} |i_{ref}|. \tag{2}$$

When applying the optimal compensation position, the Ω-synchronous component of both the input and the output of the position controller tend to zero.

IV. Suppression of Rotor Vibrations

When minimal rotor vibrations are required, the rotor can be forced to spin around its geometrical axis by applying a feed-forward current to the output of the position controller (cf. Figure 5).

In the low speed range where the poles of the state estimator are active, it is not possible to suppress the rotor vibrations by simply tuning the LQR position controller. The poles of the state estimator at 30 krpm limit the achievable performance (cf. blue curves in Figure 10 (b) and (c)), as a phase shift between rotor displacement and applied compensation current is occurring. On the other hand, a very aggressive controller would be required, resulting in poor performance or even instability.

In contrast to the feed-forward suppression of stator vibrations, both amplitude and phase of the required feed-forward currents for rotor vibration suppression

$$I_c = A_c(\Omega) \sin\big(\gamma + \varphi_c(\Omega)\big) = f(\Omega) \tag{3}$$

are a function of rotational speed and have to be stored in a look-up table, as shown in Figure 5.

The optimal feed-forward currents are found by iterative minimization of the rotor vibrations

$$I_{c,opt} = \underset{I_c}{\operatorname{argmin}} |y|. \tag{4}$$

When applying the optimal feed-forward currents, the Ω-synchronous rotor displacements tend to zero. Hence, the position controller is "disabled" at this frequency, and the Ω-synchronous component of i_{ref} is tending to zero as well.

The required current for suppression of the unbalance force and hence rotor vibrations is increasing quadratically with rotational speed

$$i_{bng,tot} = \frac{2}{3}\frac{u\Omega^2}{\chi}, \tag{5}$$

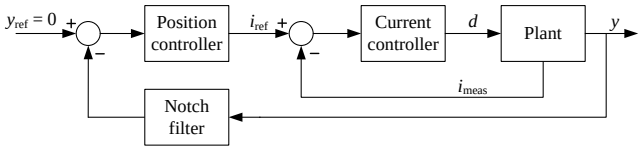

Figure 2. Control block diagram of radial rotor position control with notch filter for stator vibration suppression.

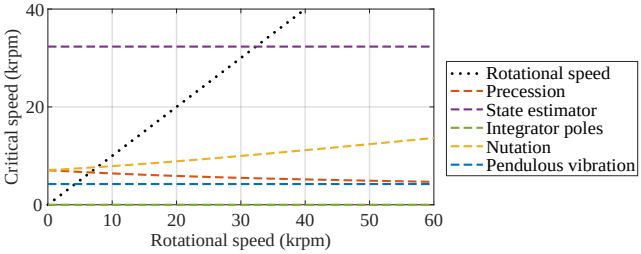

Figure 3. Campbell diagram, showing the rigid-rotor critical speeds vs. rotational speed. Ω-synchronous vibrations excite resonances at low rotor speeds.

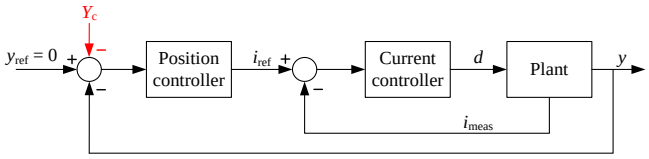

Figure 4. Control block diagram of radial rotor position control with feed forward suppression of stator vibrations.

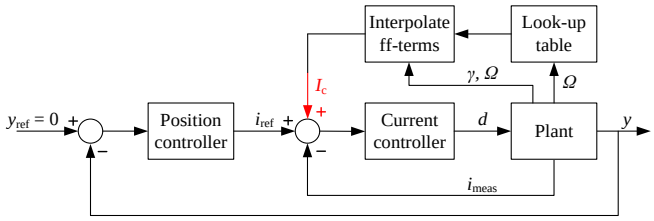

Figure 5. Control block diagram of radial rotor position control with feed-forward rotor vibration suppression.

assuming a purely static unbalance u. The magnetic bearing constant χ is relating the impressed bearing current to the resulting bearing force and depends on the properties of the windings and rotor. $i_{bng,tot}$ is describing the combined bearing current of the two bearings. Due to the quadratic relationship of $i_{bng,tot}$ on Ω, the applicability of rotor vibration suppression is limited to low rotational speeds. For the system at hand with unbalanced rotor (u = 120 mgmm, χ = 0.2 N/A, $i_{bng,tot,max}$= 3.5 A), the upper speed bound can be estimated as 28 krpm.

[4] states that balancing of the rotor and optimization of the active rotor vibration suppression are the main technological challenges for an application of the presented motor type in enhancement cavities. While the presented concept in [8] is insensitive to parallel whirls, the conical whirls resulting in a tilting of the rotational axis must be smaller than 10 µrad, corresponding to rotor tip displacements smaller than 0.35 µm for the parallel whirls.

When no rotor vibration suppression is used, the dynamic rotor unbalance must be small enough such that the resulting eccentricity per bearing is smaller than 0.35 µm. With the rotor mass of 15.7 g, this results in a maximum allowed dynamic rotor unbalance per bearing of 2.75 mgmm if no rotor vibration suppression is used.

When employing active suppression of rotor vibrations, a higher unbalance can be tolerated, and the bearing force is ensuring the rotor tip displacement is smaller than 0.35 µm. In Figure 6, the maximum allowed unbalance per bearing is shown such that the resulting unbalance force and hence rotor vibrations can be suppressed by the maximum available bearing force. The curve is calculated according to Eq. (5), using the values χ = 0.2 N/A, $i_{bng,max}$ = 4 A). Note, the value $i_{bng,max}$ is denoting the maximum allowed current per bearing, resulting in a maximum total bearing current of 4 A. This is more than previously stated in this paper. The reason is that the motor used in this paper was only passively air-cooled and did not feature temperature sensors inside the motor. When employing sensors for surveillance of the motor temperature and using improved cooling (e.g. water), a higher current can be tolerated.

At 400 krpm, an additional unbalance of 0.684 mgmm could be allowed. In other words, at 400 krpm the rotor vibrations per bearing can theoretically be reduced by 0.087 µm (cf. Figure 6), which is 25 % of the required maximum rotor vibrations of 0.35 µm.

However, very accurate position control would be required if rotor vibration suppression in the range of some tens of nm should be achieved. The limitations of the position control accuracy will be discussed in Chapter 6.

Summarized, active suppression of rotor vibrations at very high rotational speeds is not feasible for two reasons: The reduction of the rotor vibrations which can be achieved is very small at high speeds due to the limited bearing current. And even if a very small rotor unbalance is achieved such that rotor vibrations could theoretically be suppressed by the available bearing force, the rotor position would need to be measured and controlled very precisely with an accuracy in the range of some tens of nanometers.

Concluding, to meet the requirements in [4], precise balancing of the rotor is the only viable approach, with a remaining unbalance smaller than 2.75 mgmm when operating the motor at 400 krpm. In [9], a balancing method was presented achieving residual unbalances smaller than 1 mgmm.

However, at lower rotational speeds up to roughly 200 krpm, active suppression of rotor vibrations is feasible, provided a sufficient accuracy of the position control.

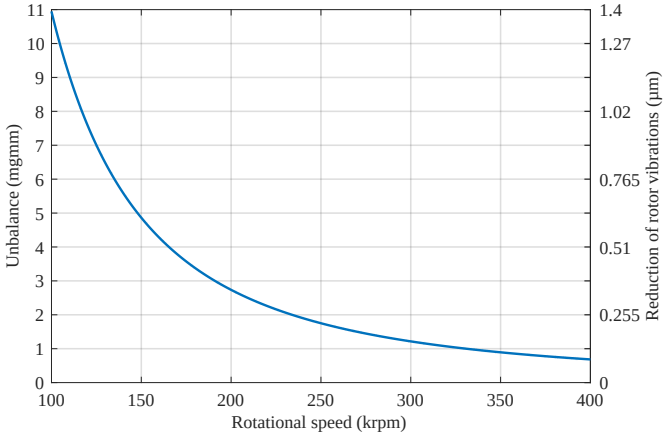

Figure 6. Physical bound on the maximum allowed rotor unbalance per bearing such that the resulting unbalance forces and hence rotor vibrations can be suppressed by the available bearing force; Corresponding reduction of rotor displacements if the unbalance force is suppressed.

V. Rotational Speed Stability

In [8], the rotational speed fluctuations of the given self-bearing motor were investigated for the first time in sufficient accuracy at rotational speeds up to 300 krpm. The investigations indicate a large potential for improvement of the rotational speed stability, and the motor drive was identified as the main source of rotational speed fluctuations, while the contribution of the radial bearing is negligible. In this paper, the speed fluctuations and motor drive system are investigated in further detail. Amongst the amplitude also the frequency of the speed fluctuations is considered, and two different modulation schemes (PWM, PAM) are compared with respect to rotational speed stability. The current control loop of the motor drive is investigated in order to identify the source of the observed rotational speed fluctuations. The considerations in this paper serve as a basis for further optimization of the drive.

A. Motor Inverter Modulation Schemes

At low rotational speeds below roughly 30 krpm, a classical pulse-width-modulation (PWM) scheme is used for generation of the rotating stator current space vector required for torque generation. Measurement of the rotor angle required for the *dq*-transformation is available by means of Hall sensors.

However, PWM is not applicable at high rotational speeds for the employed converter (CC-AMB-500). The *dq*- to abc-conversion is only performed at 10 kHz due to limited computational power on the DSP. At a rotational speed of 30 krpm, the transformation is only performed 20 times per revolution, corresponding to a resolution of the rotor angle of 18°. Hence, the approximation of the sinusoidal signal is becoming worse at high speeds, resulting in significant distortions of the motor currents.

For this reason, the modulation scheme is changed to pulse-amplitude-modulation (PAM) at higher rotational speeds. Instead of controlling the *dq*-currents directly, only the DC-link current is controlled. This current is then chopped into rectangular current blocks with a fixed length of 120°. The torque at the rotor shaft can be controlled by adjusting the value of the DC-link current and hence by adjusting the amplitude of the current pulses applied to the motor windings. Note, the employed PAM control scheme is therefore very similar to the control of an electronically commutated (brushless DC) machine, with controlling the torque by simply controlling a DC-current, which is then electronically commutated into current blocks of 120° into the corresponding phases by the inverter.

Using PAM, the input stage is acting as controlled current source and the motor inverter is commutating the current in the corresponding motor phase. Measurement of the rotor angle is no longer required, and the switching instances at the inverter are determined by the zero-crossings of the phase voltages at the motor terminals, also known as sensorless speed control.

PAM in combination with sensorless speed control is only possible above a certain threshold speed, as a sufficient back-EMF voltage is required in order to ensure proper operation of the zero-crossing detection of the phase voltages.

The main advantage of PAM in combination with sensorless speed measurement is that the scheme ensures robust operation up to very high rotational speeds while showing a modest computational effort.

VI. Experimental Verification

A. Experimental Setup

The motor CM-AMB-400 and the converter CC-AMB-500 of Celeroton AG are used for experimental verification of the presented methods.

1) Stator and Rotor Vibration Measurements

Typically, stator vibrations are measured by operating the motor on a micro vibration table (i.e. Kistler platform). However, stator vibrations can also be quantified by considering the bearing currents, resulting in a much simpler experimental setup. The force applied to the rotor, and hence the counteracting force acting on the stator, is related to the impressed *dq*- currents in the stator over the magnetic bearing constant χ

$$\begin{bmatrix} F_x \\ F_y \end{bmatrix} = \frac{3}{2}\,\chi\,\begin{bmatrix} i_d \\ i_q \end{bmatrix}. \qquad (6)$$

In the following, the total RMS radial bearing current defined as the summed RMS *dq*-currents in both hetero- and homopolar bearing is used as measure for the stator vibrations. This current is equal to the RMS DC-link current supplying the inverter stages.

For current measurement (stator vibrations), the internal current sensors on the converter are used. The rotor vibrations are measured by the eddy-current position sensors located on the sensor print in the motor. The measurement setup is shown in Figure 7.

The performance of the unbalance force rejection methods is evaluated in steps of 2 krpm for the stator vibration suppression and 1 krpm steps for the rotor vibration suppression, respectively, beginning at standstill. For each speed, the radial rotor positions and the *dq*-currents are sampled with 10 kHz over 1024 samples, which are then sent to a computer for post-processing.

2) Rotatational Speed Stability Measurement

An optical setup similar as described in [8] is used for measurement of the rotational speed fluctuations in sufficient accuracy, as illustrated in Figure 8 and shown in a photo in Figure 9. A laser beam is deflected once per revolution by a triangular prism rotor with one polished side to an optical receiver located at a distance of 1 m from the rotor. Using sequential sampling mode, a sufficient number of pulses can be sampled at the maximum sampling frequency of 400 MHz.

In [8] it was found the rotational speed fluctuations are occurring in both vacuum and air, and the relative speed fluctuations are remaining constant above 60 krpm. For these reasons, measurements are only conducted in air for rotational speeds up to 100 krpm in order to simplify the measurement setup.

B. Suppression of Stator Vibrations Measurement Results

In Figure 10 (a), the total RMS radial bearing current defined is shown over rotational speed for the different stator vibration compensations. The mean value of the *q*-current due to gravitational force is subtracted from the bearing current.
The resulting rotor vibrations, which have to be accepted in return, are shown in Figure 10 (b) and (c). The mean orbit is defined as the mean radius of the radial rotor position described in radial coordinates.

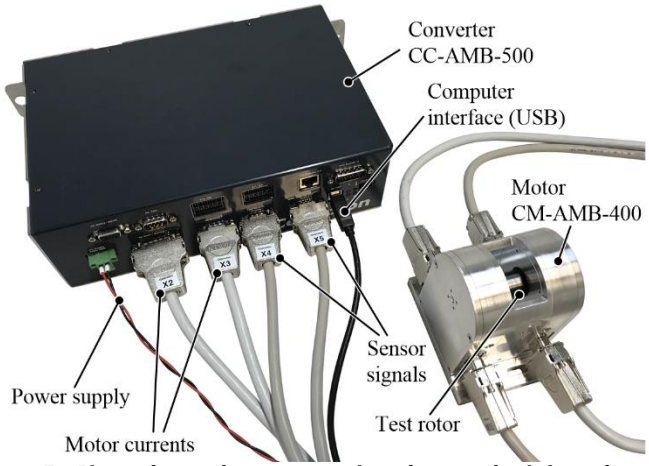

Figure 7. Photo of setup for experimental verification of unbalance force rejection.

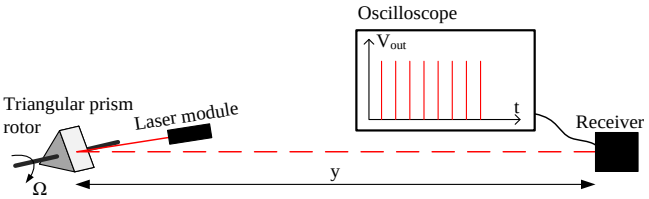

Figure 8. Setup for optical measurement of rotational speed fluctuations. Laser module: LaserComponents FP-D-635-C-F. Receiver: Broadcom AFBR-2644Z. Oscilloscope: LeCroy WaveRunner 44MXi-A.

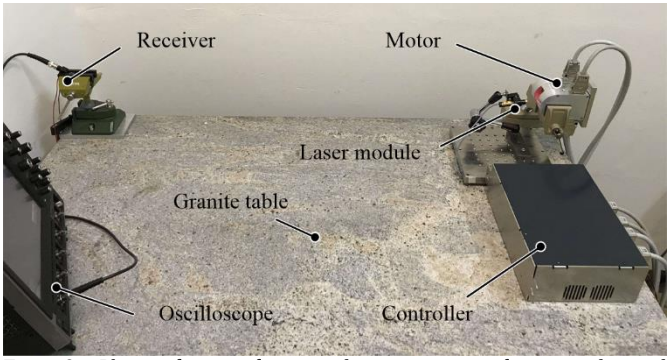

Figure 9. Photo of setup for optical measurement of rotational speed fluctuations.

The blue curves are showing the currents and rotor displacements when no suppression of stator vibrations is applied. First, the current is increasing with rotational speed as the position controller is suppressing the rotor displacements. In the range of 30 krpm an overshoot in rotor position is occurring, as the pole of Kalman filter is excited (cf. Figure 10). The position controller is applying a bearing current exhibiting a phase shift with respect to the radial rotor displacement, hence the bearing current is not suppressing but increasing the rotor vibrations. It was verified by simulations in Matlab that the overshoot of the rotor position disappears if knowledge of all system states is available and no state estimator and Kalman filter is required.

At higher speeds, both current and rotor displacements settle at a constant value. The different rotor displacements are caused by the different rotor unbalances at the two bearing locations. At high speeds, a relatively large bearing current is applied without influencing rotor position much.

When the notch filter is enabled at 60 krpm (red), a significant reduction of stator vibrations can be achieved, while the rotor vibrations remain almost unaffected. Using the feed-forward stator vibration suppression, the activation speed threshold can be lowered to standstill, while showing a similar performance as the notch filter at high speeds. The rotor displacement are even reduced in the range of 30 krpm, as the position controller is "disabled" by the feed-forward and no position overshoot due to Kalman filter is occurring.
Summarized,

- The feed-forward approach allows for significant reduction of stator vibrations up to a factor of 6 at low rotor speeds where the notch filter is not applicable.
- The controller is still able to damp Ω-synchronous disturbances/resonances and the system stability is not affected.
- The stator vibrations cannot be eliminated completely if resonances are excited at low speeds, especially for disc-like rotors, as controller still has to impress current in order to damp resonances (physical limitation).
- The notch filter is preferable at high speeds as it features a better performance and lower complexity.

C. Suppression of Rotor Vibrations Measurement Results

The peak-to-peak rotor displacements shown in Figure 11 (b) and (c) are a measure of the rotor vibrations, while the required effort for rotor vibration suppression is given by the RMS bearing current shown in Figure 11 (a). Compensation is possible up to 27 krpm, where the maximum allowed bearing current is reached.

For speeds below 15 krpm, the rotor vibrations can be reduced up to a factor of 4, while the required bearing current is even reduced slightly. This observation is confirming that the position controller is applying a bearing current space vector in the wrong direction due to the Kalman filter.

For speeds above 27 krpm, the feed-forward current is kept constant at its maximum allowed value, resulting in an increase of the rotor vibrations. The bearing current is decreasing slightly, as the position controller is increasingly responding to the rotor displacements. The output current of the position controller is showing the opposite sign of the compensation current, hence it is subtracted from the feed-forward current and the bearing current is decreasing.

The rotor vibrations can be reduced by a factor 2…3 compared to the displacements at high speeds. Above 27 krpm, the rotor vibrations start to increase, as the maximum bearing current is reached. The remaining peak-to-peak vibrations are in the range of 4 µm due to several physical limitations:

- The resolution of position sensors is 0.5 µm, as can be seen from Figure 12. Hence, the remaining rotor vibrations comport only 8 increments of the sensor.
- In Figure 9 (b) and (c), the sensor noise for disabled magnetic bearing and hence constant rotor position is marked. The peak-to-peak sensor noise is roughly 3 µm or 6 increments and hence almost as large as the remaining rotor displacements. The sensor noise level is a physical lower bound on the remaining rotor is a physical lower bound on the remaining rotor vibrations.
- The RMS value of the rotor displacements is smaller than 1 µm. However, repeatedly occurring outliers are observable, which could be caused by delays or noise in the measured rotor angle, causing a phase shift of the calculated feed-forward current.
- Also Ω-asynchronous rotor displacements are occurring, especially a 2nd harmonic component in the heteropolar

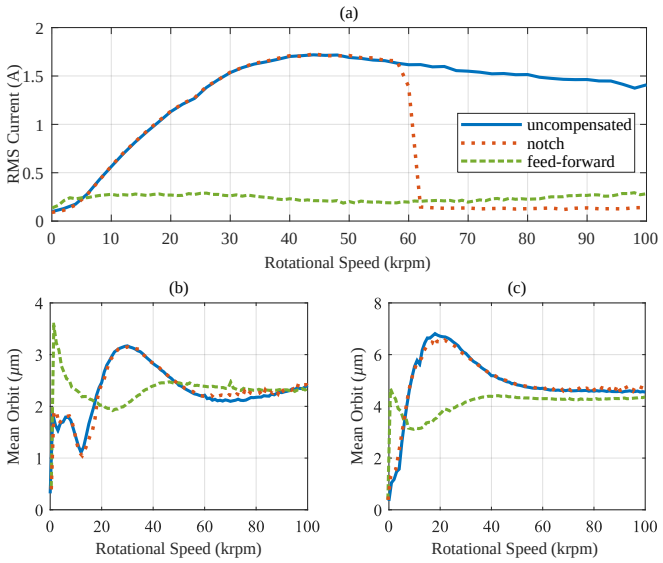

Figure 10. (a) Measurement of total mean-free RMS radial bearing current obtained by the internal current sensors, (b) measurement of mean orbit in the heteropolar and (c) homopolar bearing obtained by the internal eddy-current sensors.

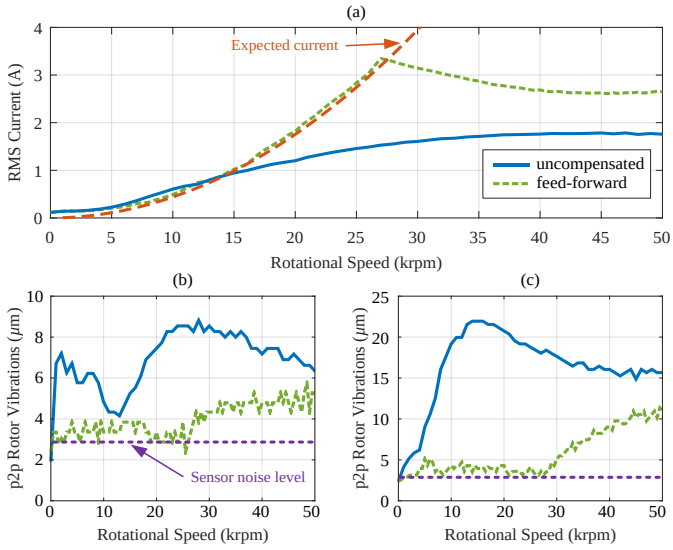

Figure 11. (a) Measurement of total RMS radial bearing current obtained by the internal current sensors, (b) measurement of maximum peak-to-peak (p2p) radial rotor displacement in the heteropolar and (c) homopolar bearing obtained by the internal eddy-current sensors. The measured noise level of the position sensors is marked in the two lower plots for comparison.

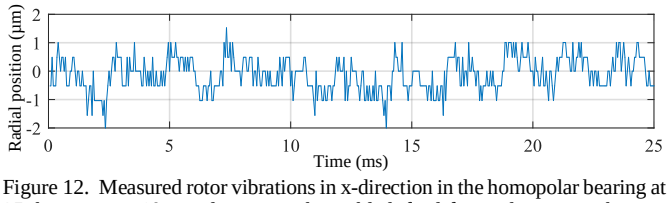

Figure 12. Measured rotor vibrations in x-direction in the homopolar bearing at 25 krpm over 10 revolutions with enabled feed-forward rotor vibration suppression. The sensor resolution of 0.5 µm is visible.

bearing caused by asymmetric bearing windings. Even though these displacements can also be suppressed by a certain extend using the feed-forward approach, some Ω-asynchronous rotor vibrations are remaining.

Concluding, the feed-forward rotor vibration suppresion is operating close the physical limits in terms of position control. In order to apply the compensation up to higher rotational speeds beyond 100 krpm or to reduce the remaining rotor vibrations, the following limitations must be overcome:

- Very accurate position measurement required: For the system at hand, peak-to–peak rotor vibrations of 4 µm can be achieved with a position sensor resolution of 0.5 µm and a sensor noise level of 3 µm peak-to-peak. To achieve the small rotor displacements required in [4], the resolution and sensor noise level of the position sensors must be improved at least by a factor 10. This imposes the biggest challenge when attempting to improve the performance of the rotor vibration suppression.
- Balancing of the rotor with residual unbalances in the range of a few mgmm is required. In [9], a method was presented capable of achieving such a high balancing accuracy.
- Very accurate measurement of the rotor angle required with low noise. May be problematic at such high rotational speeds.
- Very fast calculation of the feed-forward terms required to avoid delays.

At high speeds, the problem of a wrong rotor position estimate is no longer present. Hence, the gain of the controller could drastically be increased such that the controller is suppressing the rotor vibrations as much as possible, basically setting the penalty on the bearing current to zero such that the only goal of controller is to minimize the rotor vibrations. This could make the feed-forward compensation redundant at high speeds.

D. Rotational Speed Fluctuations Measurement Results

In Figure 13 (a), the measured deviation of the rotational period from the reference rotational period is shown. During the measurement, the motor drive was turned off, resulting in an unmodulated increase of the rotational period. The slope can be approximated by a second order polynomial and is subtracted from the measured speed fluctuations, as shown in Figure 13 (b). For the deactivated drive with subtracted slope, the contribution of air fluctuations, the magnetic bearing and measurement errors can be distinguished from the contribution of the motor drive. In [8], the same measurement was conducted in vacuum, allowing to distinguish the contribution of the magnetic bearing from the air fluctuations. It was shown the contribution of the magnetic bearing is negligible, and the motor drive is the main source of rotational speed fluctuations. From Figure 13 (b), this statement can be validated.

It can be seen the speed fluctuations for activated drive are larger than for deactivated drive when neglecting the slope, suggesting there exists a large potential for improvement of the rotational speed stability.

In Figure 14, the amplitude spectrum of the measured deviation of the rotational period from the reference rotational speed at 30 krpm is shown, basically corresponding to the spectrum of the signal in Figure 13 (b) with activated motor drive (even though the data of Figure 14 was acquired in a separate measurement over 500 revolutions). The speed fluctuations are dominated by low-frequency components below 50 Hz. The dominant harmonics are located below 50 Hz independently of the rotational speed, indicating the observed speed fluctuations are neither caused by the inverter stage nor by the sensorless speed measurement.

In Figure 15, the RMS-value of the deviation of the rotational period from the average rotational period Δt normalized with the average rotational period T_r is shown for both PWM and PAM modulation schemes. The resulting quantity is describing the relative speed fluctuations and is given in parts-per-million (ppm).

As mentioned previously, application of PWM is limited to low rotational speeds, while PAM is only applicable above a certain speed threshold in the employed system. Between 20 and 35 krpm, both schemes are applicable, allowing for direct

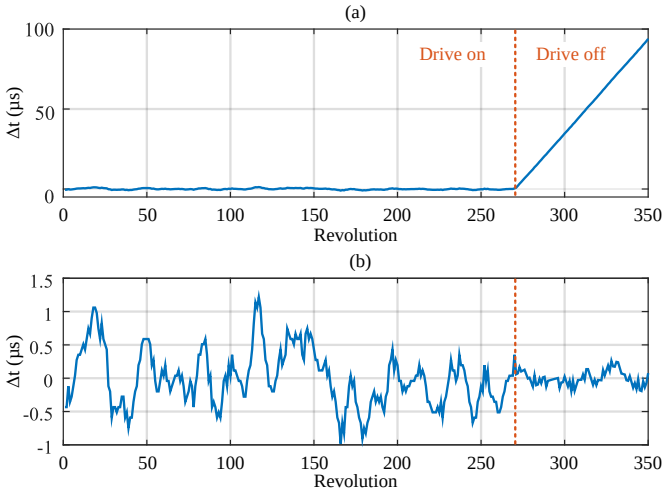

Figure 13. (a) Measured deviation of the rotational period from the average rotational period at 30 krpm for activated and deactivated motor drive and (b) subtracted slope due to unmodulated increase of the rotational period for deactivated drive (second order polynomial fit).

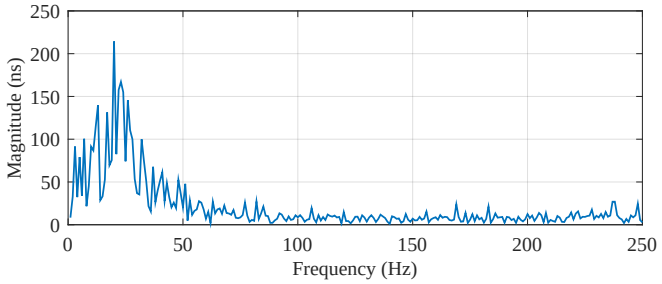

Figure 14. Amplitude spectrum of the measured deviation of the rotational period from the average rotational period at 30 krpm with activated motor drive.

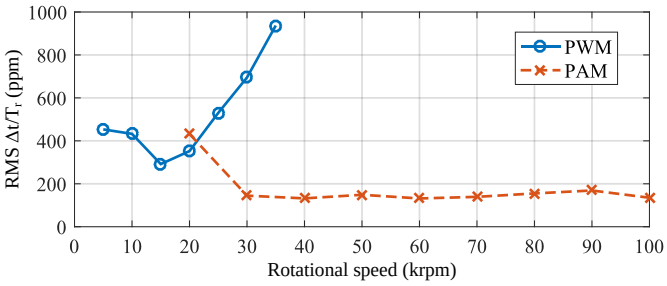

Figure 15. Measurement of RMS rotational speed fluctuations obtained by the external optical setup for PWM and PAM modulation scheme.

comparison of the resulting speed fluctuations. PAM is clearly preferable over PWM for the employed motor in terms of rotational speed stability. The limited frequency of 10 kHz at which the dq- to abc transformation is performed is causing a limited resolution of the rotor angle, causing significant distortions of the drive current with increasing rotational speed, as mentioned in chapter 4.

For a fair comparison of PWM and PAM in general, the execution frequency of the inverse *dq*-transformation has to be increased, and additionally the same measurement for the rotor angle should be used for both modulation schemes (Hall-sensor or sensorless).

For the PAM scheme, the RMS value of the *relative* speed fluctuations is roughly constant above 30 krpm (cf. Figure 15), meaning the *absolute* value of the speed fluctuations is increasing linearly with rotational speed.

Summarized, the speed fluctuations are dominated by low-frequency components of constant frequency, while the amplitude of the fluctuations is proportional to the rotational speed. When adjusting the control parameters, the frequency of the dominant speed fluctuations is shifting. The more aggressive the speed controller, the higher the frequency of the speed fluctuations. Conversely, when operating the speed control in open-loop by impressing a constant reference value of the drive current, corresponding to zero-bandwidth of the speed controller, the frequency of the speed fluctuations tends to zero, with the dominant frequency located at 2 Hz.

These observations can be explained when considering the system as linear and time-invariant (LTI). The system is showing a certain resonance at low frequencies. Adjusting the controller parameters is shifting this resonance frequency. On the other hand, the amplitude of the oscillations excited the resonance is proportional to the input applied to the system, i.e. the reference rotational speed, explaining the absolute speed fluctuations are increasing proportional to the rotational speed.

Investigation of the motor drive showed the Allegro ACS722-05AB Hall-effect current sensor used for measurement of the drive current is the main source of rotational speed fluctuations. When impressing a constant current of 0.5 A in the current sensor, the rms noise on the measured current is 40 mArms and the peak-to-peak noise even 250 mA. With lowpass-filtering, the noise can be reduced to 18 mArms, however the cutoff frequency of the filter cannot be set arbitrarily low, as the bandwidth of the speed control loop would be reduced otherwise.

The current sensor noise is containing frequency components from 1 Hz to 100 kHz, while the cutoff frequency of the lowpass filter is 10 kHz. Hence, the low-frequency noise is not filtered, and during normal operation the current controllers are responding to this noise, causing a significant ripple on the drive current. The drive current is just a few hundred milli-Amperes in the considered speed-range due to the low friction and low rotor inertia. Therefore, a current ripple of a few tens of milli-Amperes is causing torque oscillations at the rotor shaft resulting in significant speed fluctuations.

For this reason, the noise on the current measurement has to be reduced in future work in order to improve the rotational speed stability. Lowpass-filtering of the measured current is only possible to a certain extent, because a very low cutoff frequency would be required, as the sensor noise is also containing low-frequency components. The low cutoff-frequency would limit the bandwidth of the speed controller, resulting again in increased speed fluctuations.

Instead, a hardware redesign is required, employing a current sensor with a lower noise level and reduction of EMI-noise acting on the sensor signal when transferring the signal from the current sensor to the DSP.

VII. Conclusions

Above critical speeds of the rotor, both notch-filter and feed-forward approaches show comparable performance for stator force vibration suppression. However, the feed-forward approach allows lowering the activation speed to standstill. For rotor vibration suppression, the feed-forward approach shows good agreement between the calculated required forces and therefore currents for suppression of rotor displacement vibrations due to unbalance, with an inherent upper speed limit defined by the maximum current capability of the self-bearing motor and controller on the one hand, and by the unbalance of the rotor on the other hand.

Investigation of the rotational speed stability showed a large potential for improvement (factor 10), as the speed fluctuations with activated drive are larger than for deactivated drive. For a general comparison of PWM and PAM in order to determine which modulation scheme is best suited for the presented application, the limitations of the hardware, i.e. the limited computational power on the DSP, must be overcome. The employed current sensors ACS722-05AB are introducing an unacceptable amount of noise into the system, hence a redesign of the current measurement is the starting point for improvement of the rotational speed stability.

References

[1] C. Zwyssig, T. Baumgartner, J. W. Kolar, “High-speed magnetically levitated reaction wheel demonstrator,” in *Proceedings of the International Power Electronics Conference - ECCE Asia (IPEC 2014)*, Hiroshima, Japan, May 18-21, 2014.

[2] T. Stangner, H. Zhang, T. Dahlberg, K. Wiklund, M. Andersson, “Step-by-step guide to reduce spatial coherence of laser light using a rotating ground glass diffuser,” Appl Optics. 2017.

[3] B. Gerlach, M. Ehinger and R. Seiler, Low noise five-axis magnetic bearing reaction wheel, IFAC MECHATRONIC, 2006.

[4] N. Lilienfein, S. Holzberger, I. Pupeza, "Ultrafast optomechanical pulse picking," Appl. Phys. B, 2017.

[5] R. Herzog, P. Buhler, C. Gahler, and R. Larsonneur, “Unbalance compensation using generalized notch filters in the multivariable feedback of magnetic bearings,” *IEEE Transactions on Control Systems Technology*, vol. 4, no. 5, pp. 580–586, Sep. 1996.

[6] M. Hutterer, M. Schrödl, “Unbalance Compensation of a Magnetically Levitated Rotor for the Whole Operating Range,” IEEE International Conference on Mechatronics (ICM), 2017.

[7] J. Shi, R. Zmood, L. J. Qin, ”The direct method for adaptive feed-forward vibration control of magnetic bearing systems,” 7th International Conference on Control, Automation, Robotics and Vision, 2002.

[8] S. Breitkopf, N. Lilienfein, T. Achtnich, C. Zwyssig, A. Tünnermann, I. Pupeza, and J. Limpert, “Velocity- and pointing-error measurements of a 300 000 r/min self-bearing permanent-magnet motor for optical applications,” Nov 2017.

[9] E. Foremny, C. Schenck, B. Kuhfuss, “Integrated ultrasonic driven balancer for ultra precision high speed machine tools”, 3rd International Conference on System-integrated Intelligence, 2016